



# Silicon isotopic compositions of chondrule silicates in carbonaceous chondrites and the formation of primordial solids in the accretion disk

Johan Villeneuve, Yves Marrocchi, Emmanuel Jacquet

## ► To cite this version:

Johan Villeneuve, Yves Marrocchi, Emmanuel Jacquet. Silicon isotopic compositions of chondrule silicates in carbonaceous chondrites and the formation of primordial solids in the accretion disk. *Earth and Planetary Science Letters*, 2020, 542, pp.116318. 10.1016/j.epsl.2020.116318 . hal-03009515

**HAL Id: hal-03009515**

**<https://hal.univ-lorraine.fr/hal-03009515>**

Submitted on 17 Nov 2020

**HAL** is a multi-disciplinary open access archive for the deposit and dissemination of scientific research documents, whether they are published or not. The documents may come from teaching and research institutions in France or abroad, or from public or private research centers.

L'archive ouverte pluridisciplinaire **HAL**, est destinée au dépôt et à la diffusion de documents scientifiques de niveau recherche, publiés ou non, émanant des établissements d'enseignement et de recherche français ou étrangers, des laboratoires publics ou privés.

# Silicon isotope compositions of chondrule silicates in carbonaceous chondrites

Johan Villeneuve<sup>1,\*</sup>, Yves Marrocchi<sup>1</sup> & Emmanuel Jacquet<sup>2</sup>

<sup>1</sup>CRPG, CNRS, Université de Lorraine, UMR 7358, Vandœuvre-lès-Nancy, 54501, France

<sup>2</sup>IMPMC, CNRS & Muséum national d'Histoire naturelle, UMR 7590, CP52, 57 rue Cuvier,  
75005 Paris, France

Correspondence: <sup>\*</sup>johanv@crpg.cnrs-nancy.fr

## Abstract

We have determined the silicon isotopic composition of silicates (olivine and low-Ca pyroxene) in type I and type II chondrules of the carbonaceous chondrites Allende, Kaba, NWA 5959 and MIL 07342. Type I chondrule silicates show large, mass-dependent, Si fractionation with  $\delta^{30}\text{Si}$  ranging from -7 to + 2.6 ‰ whereas type II chondrule silicates are characterized by variations smaller than 2 ‰. When present, Mg-rich relict olivine grains in type II chondrules show larger Si variations than their FeO-rich counterparts. Our results show that type I chondrules are complex objects whose Si-isotopic compositions result from the legacy of precursors and SiO-rich gas-melt interactions. This corroborates that type I chondrules are nebular products and formed under open-system conditions. Our data also suggest that type II chondrules derive from their type I counterparts. This demonstrates that recycling was a common process during the evolution of the protoplanetary disk.

## 1. Introduction

The evolution of the Solar protoplanetary disk led to the formation of solids through a wide range of processes such as evaporation/condensation (Komatsu et al., 2018; Krot, 2019), fusion/crystallization (Connolly and Jones, 2016; Jacquet and Marrocchi, 2017) and collisional impacts (Krot et al., 2005). The resulting dust provided the main building blocks of asteroids and planets (Johansen et al., 2015), either in the form of refractory inclusions (i.e., CAIs = Calcium-Aluminum-rich Inclusions and AOAs = Amoeboid Olivine Aggregates), chondrules and fine-grained matrix. In theory, primordial dust should represent a powerful proxy for deciphering the conditions that prevailed in the protoplanetary disk. The translation into practice is however difficult as mineralogical, petrographic and isotopic features are commonly ambiguous, even notwithstanding secondary processes such as fluid circulation and thermal metamorphism that could have significantly blurred the messages carried by primitive meteorites (Brearley, 2006; Huss et al., 2006; Marrocchi et al., 2018a). These generally prevent straightforward interpretation and pose important uncertainties on the early times of the Solar System.

Chondrules are submillimeter-sized silicate spheroids and the favorite controversial subject of cosmochemists. This zeugma sums up the contrast between the relatively simple major mineralogy of chondrules (i.e., olivine, low-Ca pyroxene, glassy mesostasis  $\pm$  Fe-Ni metal beads) and the incalculable number of models attempting to describe their formation (see Connolly and Jones 2016 for a review). This (near)-cacophony stems from the fact that, under a relatively innocuous appearance, chondrules are complex objects whose mineralogy, textures, and chemical and isotopic compositions result from multi-step processes involving precursor recycling, melting event(s) and complex gas-melt interactions (Marrocchi et al., 2018b, 2019a; Libourel and Portail, 2018; Ebel et al., 2018). In addition, chondrule formation

likely took place for a long period of time (i.e., 4 Ma; Villeneuve et al., 2009; Bollard et al., 2017; Pape et al., 2019), in distinct reservoirs and under different conditions during the evolution of the protoplanetary disk (Jones et al., 2018). The most abundant chondrules are ferromagnesian porphyritic chondrules that can be classified to first order into type I and type II chondrules, depending of the valence state of iron (Scott and Taylor, 1983). While the limit is arbitrary defined for  $Mg\# \equiv 100 \times Mg/(Mg+Fe) = 90$ , there is a hiatus between the two, with few chondrules between  $Mg\#$  of 90 and 97 (e.g., Hertwig et al., 2018). Abundant Fe-Ni metal beads, FeO-poor silicates and volatile element depletion characterize type I chondrules whereas their type II counterparts shows FeO-rich silicates and more chondritic abundances of volatile elements. Another convenient classification is based on the modal abundance of silicates (olivine and pyroxene) in porphyritic chondrules, with PO being olivine-rich porphyritic chondrules, P pyroxene-rich and POP in between –this essentially subdivides a continuum, not to mention sectioning effects (Hezel et al., 2010).

The reduced type I chondrules have spawned drastically different formation models from planetary collisions (Faure et al., 2017) to crystallization of condensed melt (Varela and Zinner, 2018), through the incomplete melting of solid precursors (Hewins et al., 2005; Tenner et al., 2018). The recent characterization of the chemical and isotopic features of relict olivine grains suggest that type I chondrules derived from AOA-like precursors (Marrocchi et al., 2018b, 2019a), in agreement with trace element signatures (Ruzicka et al., 2007; Jacquet and Marrocchi 2017). Such models invoke gas-melt interactions with Mg- and SiO-rich gas to account for the isotopic differences observed between AOAs and the resulting chondrules (Ruzicka et al., 2007; Marrocchi et al., 2018b, 2019b). Furthermore, a protracted interaction with SiO-rich gas during chondrules formation has been invoked to explain some SiO<sub>2</sub> chemical zoning and the formation of low-Ca pyroxene shells in POP chondrules (Tissandier et al., 2002; Libourel et al., 2006; Chaussidon et al., 2008), as well as mineral chemical

zoning in palisadic olivine in PO chondrules (Libourel and Portail, 2018; Marrocchi et al., 2018b, 2019a). Considering type II chondrules, their oxidized nature compared to their reduced counterparts could either result from formation in regions with higher dust to gas ratios (Schrader et al., 2013) or lower carbon content (Connolly et al., 1994a,b). Recent experimental approach also proposed a genetic link between both types of chondrules; type II being derived from type I by oxidation (Villeneuve et al., 2015), although an independent origin is also possible (Jacquet et al., 2015a).

Silicon isotopes may provide insights into the formation conditions of both type I and type II chondrules and their potential relationship. A recent study reports that AOAs –as mentioned above, a notorious suspect as chondrule precursors (or precursor cousins)– show large, mass-dependent, light Si isotope enrichments (Marrocchi et al., 2019b). Measured bulk type I chondrules are also isotopically variable, and generally light for Si (Clayton et al., 1983; Molini-Vesko et al., 1986; Clayton & Mayeda, 1985, 1999; Georg et al., 2007; Hezel et al., 2010) potentially pointing at even larger isotopic variations at the mineral scale, perhaps comparable to those observed in AOAs. If crystallization of low-Ca pyroxene in type I POP and PP chondrules stems from protracted SiO-rich gas-melt interactions during chondrule formation, this could result in different silicon isotopic compositions between olivine and low-Ca pyroxene. Buffering by the gas for type II chondrules could result in relatively constant silicon isotopic compositions such as those recently observed in pyroxene-rich type I chondrules in enstatite chondrites (Kadlag et al., 2019), but variations might still be excepted from their common relict magnesian olivine grains possibly inherited from type I chondrules (Wasson and Rubin, 2003; Schrader et al., 2008) or the same precursors as the latter's. We thus report a comprehensive survey of the silicon isotopic compositions of type I and type II chondrules in Allende (CV3<sub>oxA</sub>), Kaba (CV3<sub>oxB</sub>) and NWA 5859 (C2-ung, CM-related). We also included isolated olivine grains (IOs) that are likely chondrule-derived (e.g., McSween

1977; Desnoyers et al., 1980; Jones 1992). We use our data to quantify the conditions of formation of these two types of II chondrules and discuss the implications on the reprocessing of primordial dust in the Solar protoplanetary disk.

## 2. Material and methods

We surveyed all chondrules in two sections of Kaba (thin sections N4075 and O229 from the Natural History Museum, Vienna, Austria), three sections of Allende (thin section Allende-4 from the Muséum national d'Histoire naturelle, Paris, France, thin sections YM1 and YM2 from CRPG), in one section of Northwest Africa (NWA) 5958 (thick section NWA 5958-1 from the Muséum national d'Histoire naturelle, Paris, France) and a thin section of Miller Range (MIL) 07342 (thick section 07342,9 from the NASA Antarctic Search for Meteorites program). Kaba is an oxidized Bali-like CV chondrite whereas Allende is the eponymous chondrite of the oxidized Allende-like CV sub-group. NWA 5958 correspond to a C2-ung CM-like chondrite, whose type II chondrule olivine Cr content as well as opaque petrography indicate minimal thermal metamorphism ( $< 300^{\circ}\text{C}$ ), yet chondrule mesostases have undergone extensive aqueous alteration, which did not affect olivine (Jacquet et al., 2016; Jacquet and Marrocchi 2017). MIL 07342 is a CO chondrite deemed of type 3.0-3.2 by the Antarctic Meteorite Petrographic Description database. Despite evidence of alteration on opaque assemblages and incipient metasomatism on chondrule mesostasis, olivine textures and compositions in chondrules show no indication of diffusional exchange. Within these three chondrites, we selected 29 porphyritic chondrules and 5 isolated olivines for determining the Si isotopes compositions of their olivine and low-Ca pyroxene crystals. This corresponds to (i) 6 type I chondrules (1 PO, 5 POP) in Kaba, (ii) 12 type I chondrules (8 PO and 4 POP), 5 type II chondrules (PO) and 2 IOs in Allende, (iii) 3 type I chondrules (2 PO, 1

POP), 1 type II chondrules (PO) and 1 IO in NWA 5958 and (iv) 2 type II chondrules (PO) and 2 IOs in MIL 07342.

Scanning electron microscope observations of chondrules were performed at CRPG-CNRS (Nancy, France) using a JEOL JSM-6510 with 3 nA primary beam at 15 kV. Quantitative compositional analyses of chondrule olivine and low-Ca pyroxene crystals were performed using a CAMECA SX-100 electron microprobe (at CAMPARIS, Sorbonne Université, Paris, France). A 150 nA focused beam accelerated to 15 kV potential difference was used for spot analyses of olivine with 20 s analysis times. The PAP software was used for matrix corrections.

We determined the silicon isotopic compositions of silicates by secondary ion mass spectrometry (SIMS) using the multi-collector CAMECA IMS 1270 E7 at CRPG. Olivines were sputtered with a ~5 nA primary  $\text{Cs}^+$  beam set in Gaussian mode and accelerated at 10 kV (Villeneuve et al., 2019). Secondary negative  $^{28,29,30}\text{Si}^-$  ions were accelerated at 10 kV and analyzed in multi-collection mode on three off-axis Faraday cups (L'2, C, and H1, respectively). Charge accumulation on the sample surface was neutralized with an electron gun. The mass resolving power was set at  $M/\Delta M = 5000$  (slit 2) to completely resolve interferences on masses 28, 29, and 30. The yields and backgrounds of the Faraday cups were calibrated at the beginning of each analytical session. Automatic centering of the transfer deflectors and mass was implemented in the analysis routine. A  $10 \times 10 \mu\text{m}^2$  raster was applied to the primary beam to ensure flat-bottomed pits. We used a set of terrestrial and synthetic standard olivine yielding Mg# ranging from 36 to 100 and a set of terrestrial standard low-Ca pyroxene with Mg# from 70 to 98 to calibrate matrix effects for Si isotopes (Villeneuve et al., 2019). Measurements typically consisted of a 90 s pre-sputtering during which backgrounds of FCs are measured, automatic mass and beam centering, and 50 cycles of 4 s integrations separated by 1 s waiting times. Thus, each measurement took ~7 min. Under these conditions,

internal precision on  $\delta^{29}\text{Si}$  and  $\delta^{30}\text{Si}$  was  $\pm 0.05$ – $0.20\text{‰}$  and  $\pm 0.10$ – $0.40\text{‰}$  ( $2\sigma$  standard error) respectively, depending on the sample and the external reproducibility on  $\delta^{29}\text{Si}$  and  $\delta^{30}\text{Si}$  for olivine and low-Ca pyroxene standards was  $\pm 0.12\text{‰}$  and  $\pm 0.21\text{‰}$  respectively ( $2\sigma$  standard error).

### 3. Results

Olivine and low-Ca pyroxene in chondrules and isolated olivines investigated herein show Mg# in the range 44.6 - 99.9 and 90 - 99.2 respectively (Supplementary table S1). A total of 644 individual Si isotopes analyses were performed among the 29 chondrules and 5 isolated olivines. Since the data (reported in table S1 and plotted in Fig. 1) fall on a mass-dependent fractionation line ( $\delta^{29}\text{Si} = 0.511 \times \delta^{30}\text{Si}$ ), we will only discuss  $\delta^{30}\text{Si}$  values in the following. Overall, the silicon isotopic composition in chondrule olivine and low-Ca pyroxene show large variations, up to  $\sim 5\text{‰}$  per amu, with  $\delta^{30}\text{Si}$  values ranging from -4.5 to 1.9 ‰ in Allende, from -7.0 to 1.2 ‰ in Kaba, from -6.9 to 2.6 ‰ in NWA 5958 and -1.9 to 0.8 ‰ in MIL 07342 (Fig. 1, table S1). Isotopic compositions in 4 type I POP chondrules from Allende reveal systematically lighter compositions of low-Ca pyroxene compared to olivine from the same chondrule, with an average shift of  $\delta^{30}\text{Si}$  values comprised between 0.3 and 1.2 ‰ (Fig. 2, Table 1). Furthermore,  $\delta^{30}\text{Si}$  values of low-Ca pyroxene show a narrow range of variation compared to olivine from the same chondrule (Fig. 2, Table 1, Supplementary table 1). Among the olivine grains, we identified relicts, whether as Mg-rich olivine in type II chondrules or Ti-Al-poor olivine with oxygen isotope compositions deviating from host olivine in type I chondrules (as measured by Marrocchi et al., 2018b, 2019a). Relicts in 1 Allende chondrule, 3 Kaba chondrules and 5 NWA 5958 chondrules do not show any systematic  $\delta^{30}\text{Si}$  shift (nor any correlation) relative to host olivines (Table 1)



with possibly more (intra-chondrule) variability. Notwithstanding relicts, the most extreme  $\delta^{30}\text{Si}$  values tend to lie in the outer olivine grains in type I chondrules (Fig. 3). However, the behavior of Si isotopic composition varies strongly with the Mg# of olivine. It indeed yields  $\sim 10$  ‰ variations of  $\delta^{30}\text{Si}$  values (up to  $\sim 6$  ‰ within a single chondrule) in Mg-rich olivine, i.e. in type I chondrules, but variations smaller than 2 ‰ in Fe-rich olivine, i.e. in type II chondrules (Fig. 4, Table S1). Even though  $\delta^{30}\text{Si}$  values in MgO-rich olivine are scattered toward extreme values, the chondrule averages span ranges similar (if extended to  $\sim 1$  ‰ lighter compositions) to their FeO-rich counterparts (Fig. X) and the grand average is only marginally lighter ( $-0.89 \pm 1.41$  ‰ (1SD) vs.  $-0.31 \pm 0.57$  ‰ (1SD) respectively). This is within range of variations previously observed for bulk chondrules (Fig. 5, Clayton et al., 1983; Molini-Vesko et al., 1986; Clayton & Mayeda, 1999; Georg et al., 2007; Hezel et al., 2010).

## 4. Discussion

### 4.1 Origin of type I chondrules

More than two centuries after their first description by Jacques Louis de Bournon in 1802, the origin of chondrules is still the subject of an intense debate. Over time, nebular and planetary theories have experienced ups and downs that led to the development of drastically different models attempting to explain their peculiar characteristics (Connolly and Jones, 2016). Our results reveal that Mg-rich olivine grains registered large mass-dependent silicon isotope variations that can reach up to  $\sim 6$  ‰ in  $\delta^{30}\text{Si}$  within a single type I chondrule (Figs. 1, 4; Table S1). These results are at odds with the very limited Si-isotopic fractionation (a few tenths of permil at most, e.g. Savage et al., 2014) expected in models where chondrule

olivines would result from the crystallization of (i) closed-system magma droplets in regions with extreme dust/gas ratios (Alexander et al., 2018) or (ii) magma ocean-like environments in fully or partially molten differentiated planetesimals (Faure et al., 2017). Furthermore, the latter scenario is not supported by the large *mass-independent* oxygen isotope variations commonly reported in type I chondrules (e.g. Ushikubo et al., 2012; Marrocchi et al., 2018b, 2019a; Tenner et al., 2018) as magmatic processes would only produce sub-permil *mass-dependent* O-isotope variations (Richet et al., 1977; Eiler et al., 2001). Our results thus raise the question of the origin of the isotopic variability observed in chondrules for major rock-forming elements such as Si and O. Based on trace element and oxygen isotope features of olivine grains, it has been recently proposed that relict olivine grains in type I chondrules were inherited from AOA-like precursors (Marrocchi et al., 2018b, 2019a). In addition, similarly to chondrules Mg-rich olivines, AOA olivines show large, mass-dependent, light Si isotope enrichments (Marrocchi et al., 2019b), with  $\delta^{30}\text{Si}$  ranging from  $-9\text{‰}$  to  $-1\text{‰}$ . These are also seen in the relicts analyzed herein (Fig. 6–7). Taken together, this suggests that isotopic features of Mg-rich olivine in type I chondrules reflect (i) the legacy of the precursor isotopic variabilities and (ii) the important role of gas-melt interaction during chondrule formation.

Relict and host olivines previously characterized for O-isotopes display very similar Si-isotope distributions (Fig. 7; Marrocchi et al., 2018b, 2019a). No specific correlation was observed between trace elements abundances and  $\delta^{30}\text{Si}$ , and thus between  $\Delta^{17}\text{O}$  and  $\delta^{30}\text{Si}$  in relict and host olivine grains (Fig. 8). Considering AOAs as plausible chondrule precursors, this lack of correlation, for the relicts, likely results from the large intrinsic Si-isotope heterogeneities observed in AOAs (Marrocchi et al., 2019b) despite their relative O-isotope homogeneity (Krot, 2019). Such decoupling between Si and O-isotope behaviors in AOAs is not surprising since they resulted from different processes one mass-dependent, and the other

mass-independent: condensation for the former and variable exchange with later  $^{16}\text{O}$ -poor gas for the latter.

## **4.2 Gas-melt interaction during type I chondrule formation**

The question of gas-melt interactions is of the utmost importance as growing evidence suggests that chondrule formation took place under non-canonical conditions with enhanced partial pressure of condensable species such as alkali oxides (Tissandier et al., 2002; Krot et al., 2006; Libourel et al., 2006; Fedkin & Grossman, 2013; Marrocchi & Libourel 2013; Piani et al., 2016). Chondrule formation in such environment must result in strong Si and O isotopic exchanges with the gas since Si and O isotopic compositions of chondrules.

The clustering of host olivine grains around the same  $\Delta^{17}\text{O}$  suggests that the chondrules readily exchanged oxygen isotopes with the gas after melting, and were buffered at the oxygen isotopic composition of their formation region (e.g., Marrocchi et al., 2018b, 2019a). Approach to isotopic equilibrium is supported by limited Si isotopic variations (close to bulk carbonaceous chondrite compositions) in host olivine grains from chondrule interiors.

The more variable Si isotopic compositions seen in the exterior of "palisades" (Libourel and Portail, 2018) however suggest some kinetic effects. Recent studies based on cathodoluminescence and high-current X-rays maps have invoked that those grains grew asymmetrically toward the exterior as a result of SiO and Mg dissolution onto the melt (Libourel and Portail, 2018; Marrocchi et al., 2018b, 2019a). The condensation of SiO may have taken place under some level of supersaturation, hence a light isotope enrichment first, but as the residual gas became (by mass balance) isotopically heavier, later increments of olivine would have been heavier, hence the two extremes seen in these olivines.

Open-system behavior does not stop with olivine. Laboratory experiments have shown that low-Ca pyroxene shells can form in chondrule melts by incorporation of SiO from the nebular gas, during the partial dissolution of olivine precursors (Tissandier et al., 2002). Since host olivine and low-Ca pyroxene would have formed from a melt buffered by the ambient gas (itself largely due to evaporation of chondrule precursors), both should carry the same  $\Delta^{17}\text{O}$  as generally observed (Ushikubo et al., 2012, Tenner et al., 2013, 2015, 2018) despite contrary earlier results by Chaussidon et al (2008). Still, olivine tends to have  $\delta^{18}\text{O}$  higher by  $\sim 1\text{‰}$  than co-existing phases in CO and CR chondrites (Tenner et al. 2013, 2015, 2018), which these authors ascribed to kinetic (mass-dependent) effects during evaporation/recondensation. Our data show the same phenomenon for silicon isotopes with the measured average difference (0.3-1.2 ‰; Fig. 2) well in excess of the  $<0.1\text{‰}$  equilibrium fractionation predicted at equilibrium at 1700 K (Méheut et al., 2009). Such  $^{28}\text{Si}$  enrichments of low-Ca pyroxene shells have been previously observed in CR and CV chondrules and ascribed to near-equilibrium condensation of Si from a  $\text{SiO}_{(\text{g})}$  with partial pressure slightly higher than the equilibrium partial pressure of SiO (Harju and Young, 2013; Harju et al., 2015). This, however, represents a break from the heavy signatures seen in some palisadic olivine analyses, as the residual SiO gas would have been isotopically heavier than it was when these grains were growing. This could be overcome by invoking a higher supersaturation at that stage, as a result of an increased cooling rate. Rapid cooling of order of 100-1000 K/h are suggested by the large proportion of monoclinic enstatite (e.g., Soulié, 2014), at variance with the days suggested by Ca diffusion in interior olivines (e.g., Marrocchi et al., 2018b). Non-linear chondrule cooling histories invoking quenching after a subisothermal phase have been already proposed (Jacquet et al., 2013, Villeneuve et al., 2015; Libourel and Portail, 2018). The palisadic olivine discussed above may then correspond to an intermediate stage in this cooling acceleration. Late supersaturation of  $\text{SiO}_{(\text{g})}$  would explain

the marginally lighter Si isotopic composition of type I chondrules compared to the whole-rock carbonaceous chondrite (e.g., Dauphas et al., 2015).

#### **4.3 The link between type I and type II chondrules**

While they are more abundant in ordinary chondrites, type II chondrules are also commonly observed in carbonaceous chondrites (Fig. 6; Scott & Krot, 2014). Although they have spawned fewer competing models than their type I counterparts, they remain controversial as well. In the early nineties, on the basis of petrographic, mineralogical and chemical observations and also experiments, type II chondrules were interpreted as closed-system fractionally crystallized droplets heated at near-liquidus temperatures and cooled at ~1-500 K/h (e.g. Jones, 1990; Radomsky and Hewins, 1990; Jones and Lofren, 1993; see also review by Jones et al., 2018). Although open- vs. closed-system chondrule formation has been strongly debated, most observations point toward important gas-melt interactions and therefore non-canonical nebular environments of formation (see for instance review by Ebel et al., 2018). The important concentrations of volatiles and moderately volatile elements (i.e., Na, K, Mn, Cr, Sr and Fe) and the larger average size type II chondrules compared to type I chondrules were used as arguments for type II chondrule formation (i) as the precursors of type I chondrules, which would formed *via* high-temperature reduction and evaporation processes (Hewins et al., 2005; Ruzicka et al., 2008, 2012) or (ii) in a different nebular (sub)reservoir than that at the origin of type I chondrules (e.g. Jones, 2012; Hewins & Zanda, 2012; Jacquet et al., 2015a). On the other hand, recent chemical and isotopic observations have suggested that type II chondrules were derived from type I chondrules via high-temperature oxidation and protracted gas-melt interactions (Connelly et al., 2008, Ruzicka et al., 2008, Schrader et al., 2008). A comprehensive experimental approach proved that such

process is feasible and succeeded in reproducing many type II chondrules features, such as chemical zonings in olivine and the preservation of Mg-rich olivine relics (Fig. 6; Villeneuve et al., 2015).

Our results show that FeO-rich olivine in type II chondrules are characterized by more homogeneous Si isotope compositions compared to type I chondrules (Figs. 4, 5). This could be taken as a supporting closed-system crystallization. However, the silicon isotopic heterogeneity observed within type II chondrules containing Mg-rich olivine relics (Fig. 6, Table S1) necessarily implies a formation of their precursors under open-system conditions. As their variability mimics that of type I chondrules (Fig. 6, Table S1), these could have been derived from reduced type I chondrules. This would indicate a genetic link between type I and type II chondrules as already proposed based on the observational and experimental evidence (Connelly et al., 2008, Ruzicka et al., 2008, Schrader et al., 2008, Villeneuve et al., 2015). If correct, this would imply that type II chondrules experienced important gas-melt interactions; at least for volatile elements that would have been substantially enriched.

## **5. Concluding remarks**

We have determined the silicon isotope compositions of silicates (olivine and low-Ca pyroxene) in type I and type II chondrules in the carbonaceous chondrites Allende (CV3<sub>oxA</sub>), Kaba (CV3<sub>oxB</sub>), NWA 5958 (C2-ung) and Miller Range (MIL) 07342 (CO). Our main results are:

- 1- Type I chondrule silicates are characterized by large, mass-dependent, silicon isotope variations with  $\delta^{30}\text{Si}$  ranging from -7 to + 2.6 ‰. Low-Ca pyroxene crystals define a narrow range of isotopic values and show systematically lighter Si isotope compositions compared to olivine grains.

2- Type II chondrule FeO-rich silicates show Si isotope variations smaller than 2 ‰. When present within type II chondrules, Mg-rich relict olivine grains exhibit larger Si isotope variations than their FeO-rich counterparts.

From this, we drew the following inferences:

1- As magmatic processes would only generate Si-isotope fractionation at a level of few tenths of permil, this implies that type I chondrules could result neither from the crystallization of closed-system magma droplets under extreme dust/gas ratios nor from the crystallization of molten differentiated planetesimals.

2- Si-isotope composition of type I chondrules represent the legacy of the precursor isotope variabilities and kinetic effects during gas-melt interactions, possibly as a result of accelerated cooling near the end of olivine crystallization and during pyroxene formation. This supports models where type I chondrules results from the recycling of AOA-like precursors.

3- The Si isotope heterogeneity observed within type II chondrules containing Mg-rich olivine relics implies a formation of their precursors under open-system conditions. This also supports models where type II are derived from type I chondrules *via* drastic changes in the oxidation conditions.

## Acknowledgments

The authors are grateful to Nordine Bouden for his assistance with isotopic measurements. We also thank the Muséum national d'Histoire naturelle (Paris, France), the Natural History Museum of Vienna (Austria) and the Antarctic Search for Meteorites (ANSMET) program for loaning samples. US Antarctic meteorite samples are recovered by ANSMET that has been funded by NSF and NASA, and characterized and curated by the Department of Mineral Sciences of the Smithsonian Institution and Astromaterials Curation. This work was funded by l'Agence Nationale de la Recherche through grant ANR-18-CE31-0010-01 CASSYSS (PI Johan Villeneuve). This is a CRPG contribution #2729.



## Figure captions

Fig.1: Three silicon-isotope diagram plot of all individual analyses performed by SIMS in olivine and low-Ca pyroxene from the 21 type I (in red, n=467), 8 type II (in blue, n=133) chondrules and 5 IOs (in green, n=44) studied. The data show a large range of mass-dependent fractionation from  $\sim -7\text{‰}$  to  $\sim 2.5\text{‰}$ . Error bars are 2 SE

Fig.2: Average  $\delta^{30}\text{Si}$  compositions of MgO-rich olivine and low-Ca pyroxene in four POP chondrules from Allende showing a systematic shift of low-Ca pyroxene toward lighter compositions by  $\sim 0.3 - 1.2 \text{‰}$ . As shown by the error bars (1 SD) low-Ca pyroxene compositions are less scattered than MgO-rich olivine compositions.

Fig.3: Representative chondrules and the Si isotopic composition of their olivines, (A) Kaba N4075 - Ch11 and (B) NWA 5958 - Ch1. SIMS measurements are indicated by ellipses whose colors vary with the Si isotopic composition.

Fig. 4: Silicon isotopic composition of olivine and low-Ca pyroxene crystals of type I and type II chondrules from NWA 5958 (C2-ung), MIL 07342 (CO), Kaba (CV3<sub>oxB</sub>) and Allende (CV3<sub>oxA</sub>) plotted against their respective Mg contents. Type I chondrule silicates show larger isotopic variabilities than type II chondrule silicates characterized by near-constant  $\delta^{30}\text{Si}$ . The light brown area indicates bulk silicon isotopic compositions from literature (Clayton et al., 1983; Molini-Vesko et al., 1986; Clayton & Mayeda, 1999; Georg et al., 2007; Hezel et al., 2010).

Fig. 5: Curves show probability density function of  $\delta^{30}\text{Si}$  of type I and type II chondrule silicates (olivine and low-Ca pyroxene) from NWA 5958 (C2-ung), MIL 07342 (CO), Kaba (CV3<sub>oxB</sub>) and Allende (CV3<sub>oxA</sub>).

Fig. 6: Curves show probability density function of  $\delta^{30}\text{Si}$  of relict and host olivine grains inferred from previous oxygen isotope compositions (Marrocchi et al., 2018b, 2019a). No specific Si isotope difference is observed between relict and host olivine grains.

Fig. 7: Diagram showing  $\Delta^{17}\text{O}$  versus  $\delta^{30}\text{Si}$  of relict and host olivine grains (distinguished from previous oxygen isotope compositions; Marrocchi et al., 2018b, 2019a) in Kaba and NWA 5958. The absence of correlation suggests that different cosmochemical processes control oxygen and silicon isotope compositions.

Fig. 8: (A) Back-scattered electron image of a FeO-rich type II chondrule from Allende-YM1 showing relict Mg-rich olivine grains. (B) Silicon isotopic composition of FeO- and Mg-rich olivine grains. Mg-rich olivine grains show larger isotopic variability than FeO-rich olivine crystals. The light blue area indicates bulk silicon isotopic compositions from literature (Clayton et al., 1983; Molini-Vesko et al., 1986; Clayton & Mayeda, 1999; Georg et al., 2007; Hezel et al., 2010).

430 Table 1: Average  $\delta^{30}\text{Si}$  and Mg# of chondrules and isolated olivines (IOs) from Allende,  
 431 Kaba, NWA 5958 and MIL 07342 studied. Mg Ol. = Mg-rich olivine, low-Ca Px. = low-Ca  
 432 pyroxene, Fe Ol. = FeO-rich olivine. Relict are either Mg-rich olivines enclosed in FeO-rich  
 433 olivines in type II chondrules or Mg-rich olivines with O isotopic compositions different from  
 434 host olivines (see Marrocchi et al., 2018, 2019). N is the number of individual analyses.  
 435 Errors are one standard deviation.

name	type	Mineral	$\delta^{30}\text{Si}$ av	1 SD	Mg# av	1 SD	N
All YM2-Ch13-1	I POP	Mg Ol.	0.60	0.56	98.13	2.97	12
		low-Ca Px.	0.10	0.44	94.75	1.11	7
All YM2-Ch13-2	I POP	Mg Ol.	0.51	0.74	91.98	2.82	10
		low-Ca Px.	-0.47	0.67	94.96	0.35	3
All YM2-Chc2	I PO	Mg Ol.	-0.59	0.76	92.12	3.91	16
All YM2-Ch20	I POP	Mg Ol.	-0.66	0.62	93.23	1.92	11
		low-Ca Px.	-0.94	0.40	94.26	1.74	8
All YM2-Ch6	I PO	Mg Ol.	-1.23	0.95	98.16	2.43	19
All YM2-Ch27	I PO	Mg Ol.	-0.41	0.52	99.12	1.54	31
All YM2-Ch24	I PO	Mg Ol.	0.44	0.79	97.87	1.40	16
All 4-Ch36	I PO	Mg Ol.	0.12	1.00	95.56	1.76	18
All 4-Ch32	I PO	Mg Ol.	0.53	0.84	96.30	2.00	20
All 4-Ch40	I PO	Mg Ol.	0.10	0.87	96.99	2.67	21
All 4-Ch31	I PO	Mg Ol.	-2.02	0.49	99.22	0.64	10
All 4-Ch39-2	IO	Mg Ol.	-2.45	1.35	93.10	11.77	6
All YM1-Ch18	I POP	Mg Ol.	-1.34	1.04	95.59	0.40	3
		low-Ca Px.	-2.51	0.44	98.76	0.34	5
All YM2-Ch15	II PO	Fe Ol.	-0.03	0.48	65.80	4.52	25
All YM2-Ch23	II PO	Fe Ol.	0.00	0.27	52.17	3.55	7
All YM2-Ch9	II PO	Fe Ol.	-0.40	0.20	75.79	5.51	14
All YM2-Ch14	IO	Fe Ol.	-0.76	0.39	68.53	4.20	11
All YM1-Ch5	II PO	relict Mg Ol.	-1.42	1.53	89.28	3.08	25
		Fe Ol.	-0.65	0.53	69.69	6.24	7
All YM2-Ch5	II PO	Fe Ol.	-0.27	0.40	89.58	1.44	23
Kaba N4075-Ch11	I PO	relict Mg Ol.	-1.54	1.48	98.59	0.25	3
		host Mg Ol.	-1.55	0.97	98.63	0.08	17
Kaba N4075-Ch18	I POP	relict Mg Ol.	-5.57	-	96.28	-	1
		host Mg Ol.	-1.85	1.90	96.06	0.44	6
Kaba N4075-Ch25	I POP	host Mg Ol.	-0.88	1.12	99.29	0.42	26
Kaba N4075-Ch1	I POP	host Mg Ol.	-1.66	1.53	98.69	0.48	43

Kaba N4075-Ch12	I POP	host Mg Ol	-0.60	1.12	98.71	0.23	37
Kaba 0229-Ch1	I POP	host Mg Ol	0.21	0.64	98.50	0.37	4
		relict Mg Ol.	-1.82	1.45	98.58	0.06	6
NWA 5958-Ch1	I PO	relict Mg Ol.	-1.12	0.99	99.39	0.03	13
		host Mg Ol	-1.56	1.42	99.36	0.12	33
NWA 5958-Ch7	I PO	relict Mg Ol.	-1.29	2.34	99.26	0.03	4
		host Mg Ol	-1.56	1.49	99.28	0.07	41
NWA 5958-Ch2	I POP	relict Mg Ol.	-2.27	2.28	95.11	0.32	3
		host Mg Ol	-0.53	1.98	95.09	0.36	20
NWA 5958-Ch20	II PO	relict Mg Ol.	-1.89	0.55	96.22	0.46	4
		Fe Ol.	0.55	0.36	62.77	6.89	2
NWA 5958-IO-A	IO	Fe Ol.	-1.39	0.27	70.10	2.75	10
MIL 07342-ChB	II PO	Fe Ol.	0.11	0.48	81.87	4.76	11
MIL 07342-ChA	II PO	Fe Ol.	0.20	0.31	54.57	5.32	15
MIL 07342-ChC	IO	Fe Ol.	-0.29	0.29	81.64	4.29	12
MIL 07342-ChD	IO	Mg Ol.	-0.94	0.61	99.31	0.24	5

436

437

438

439

440

441

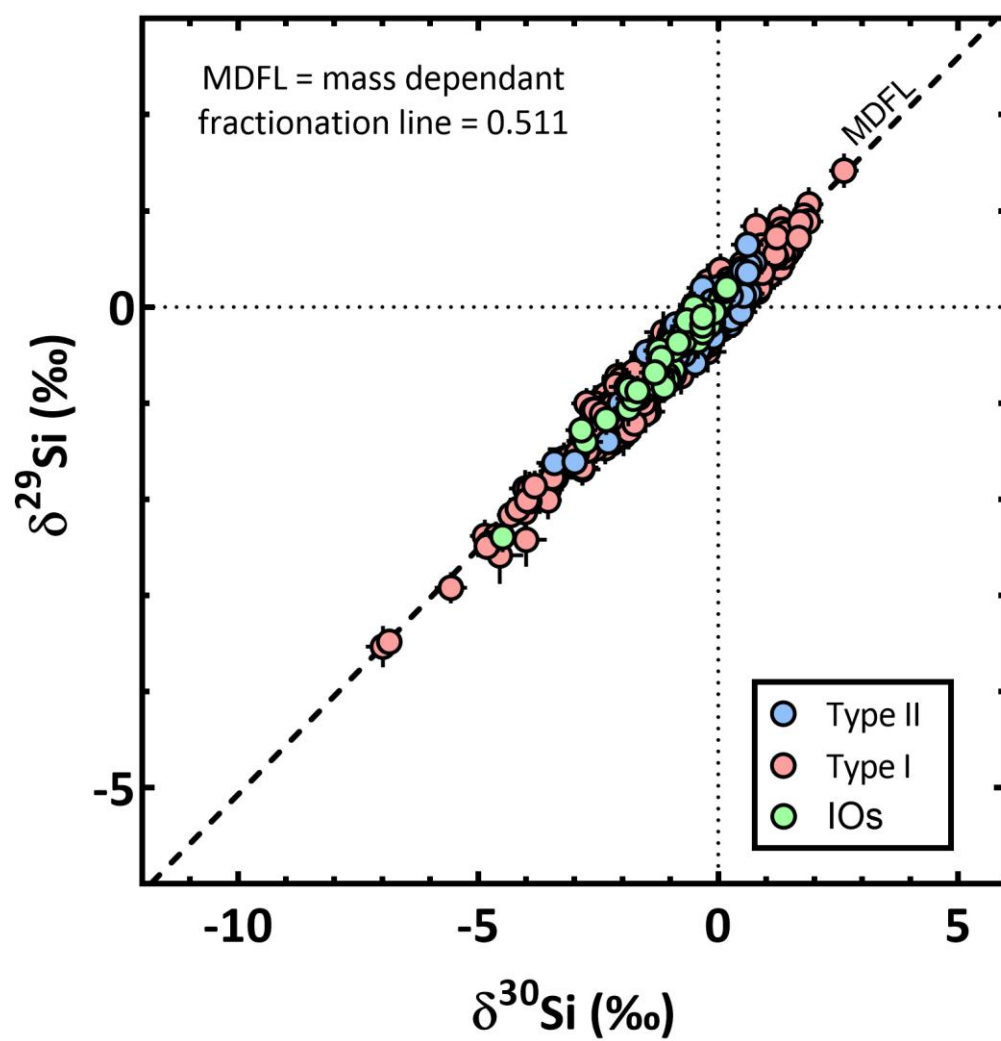
442

443

444

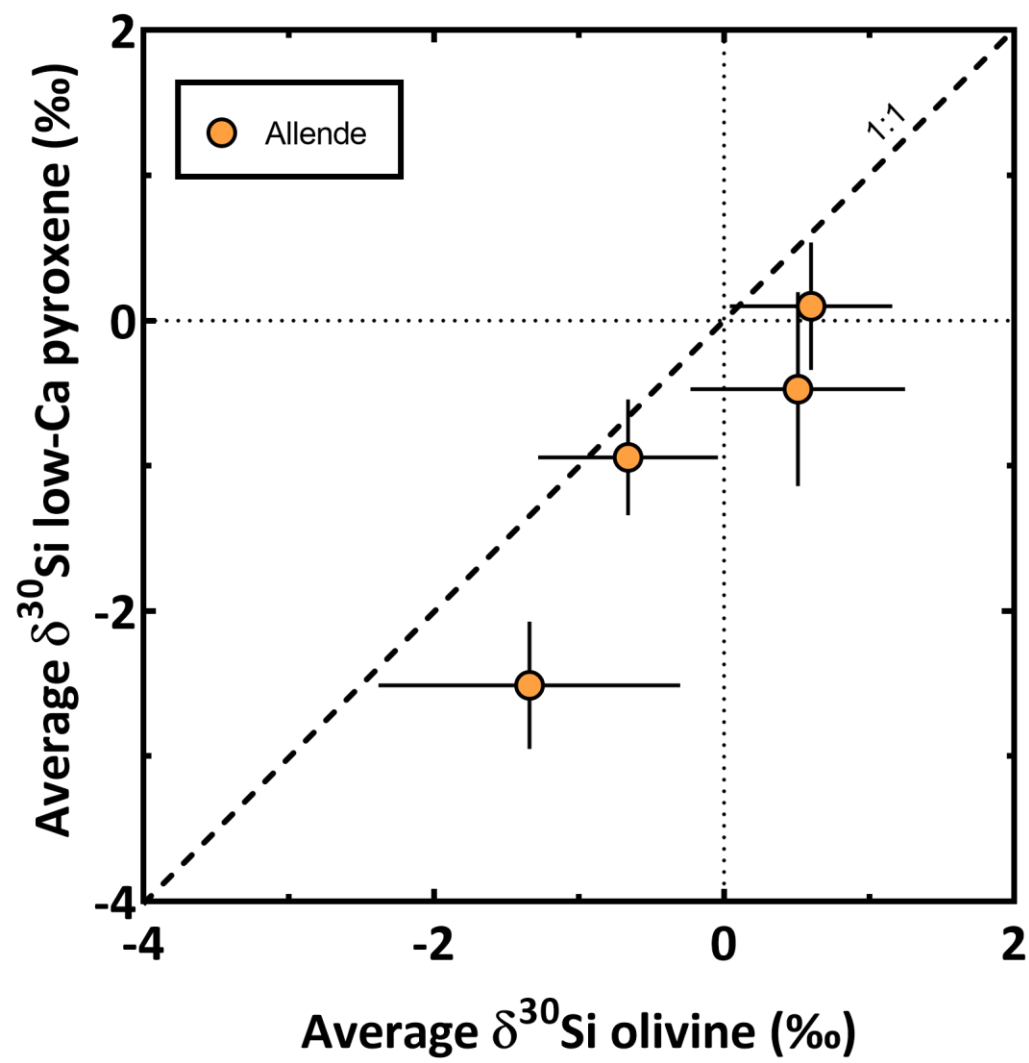
445

446 Fig. 1



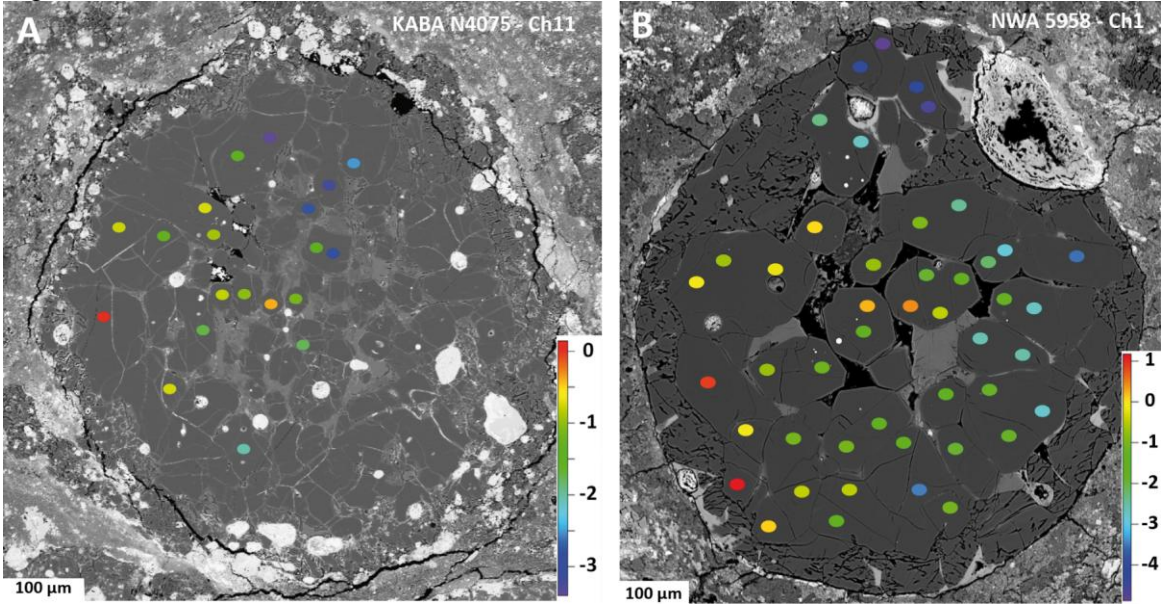
447  
448  
449

450 Fig.2

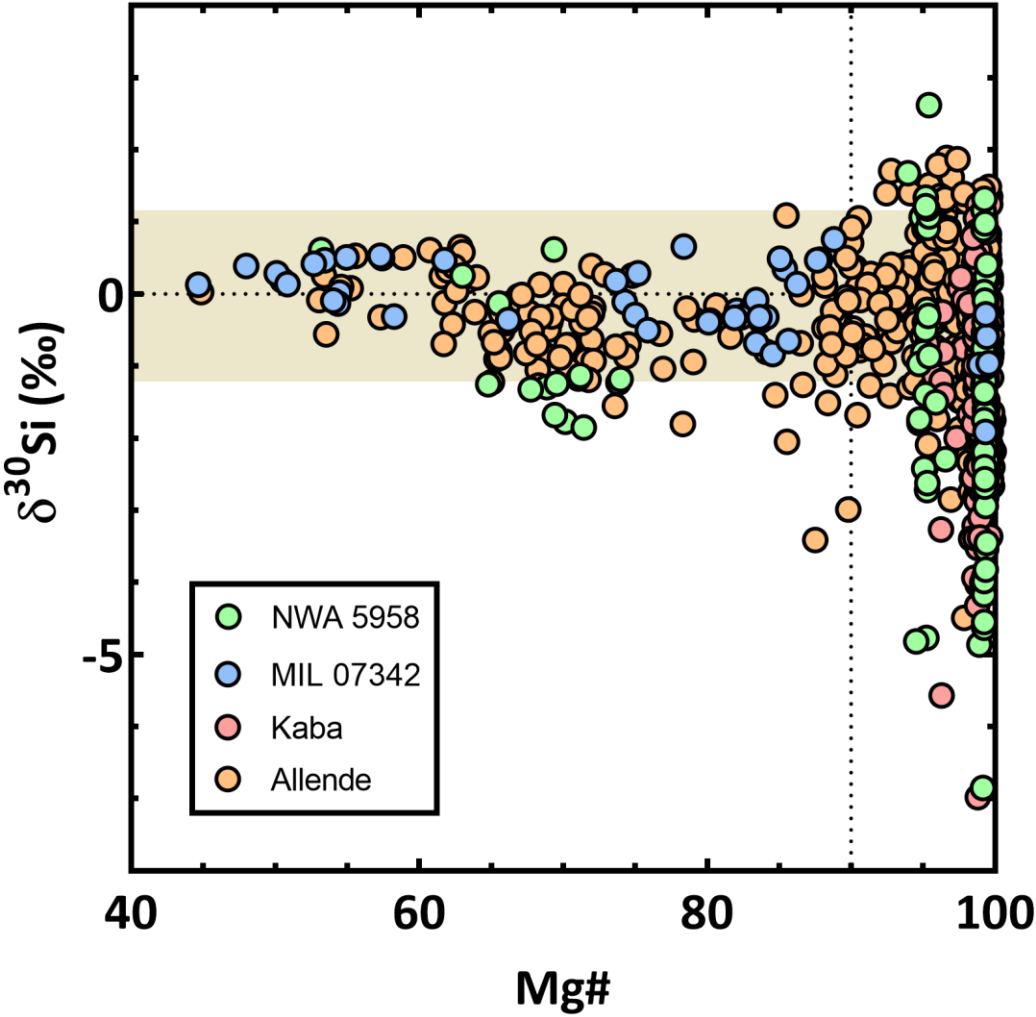


451  
452  
453  
454

Fig. 3

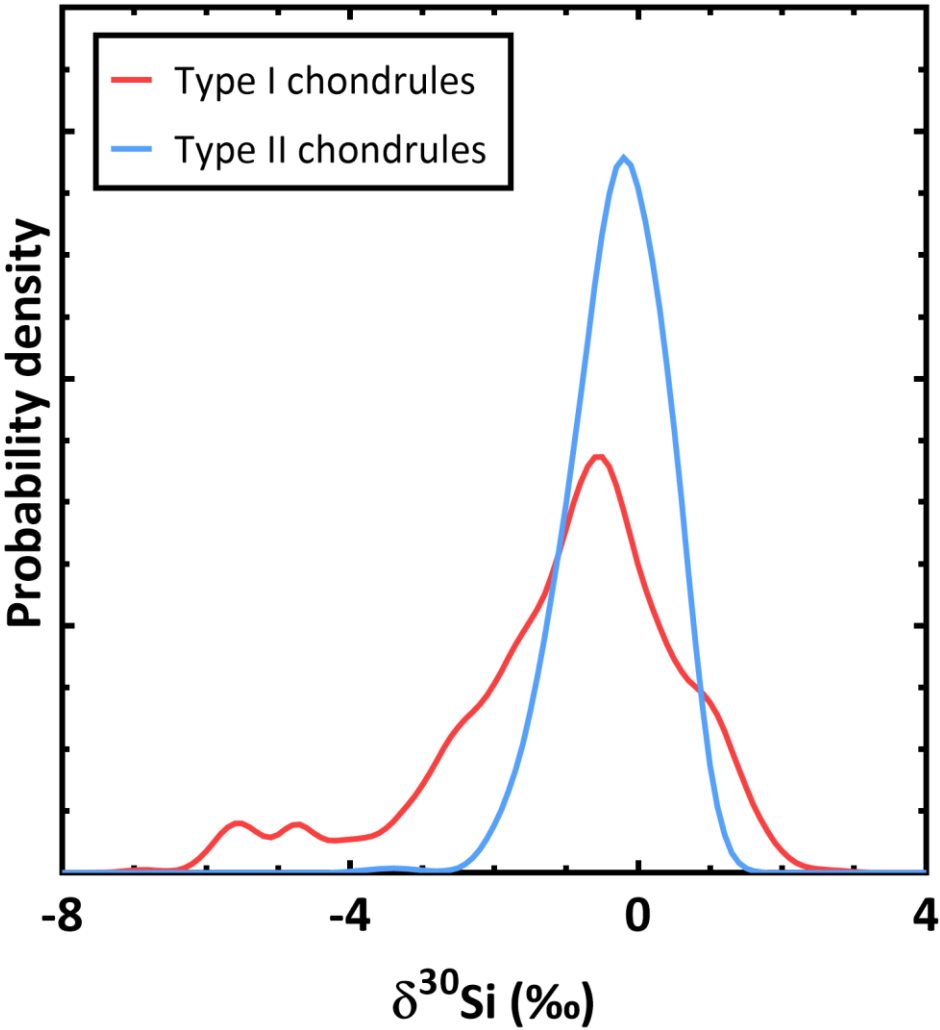


460 Fig. 4



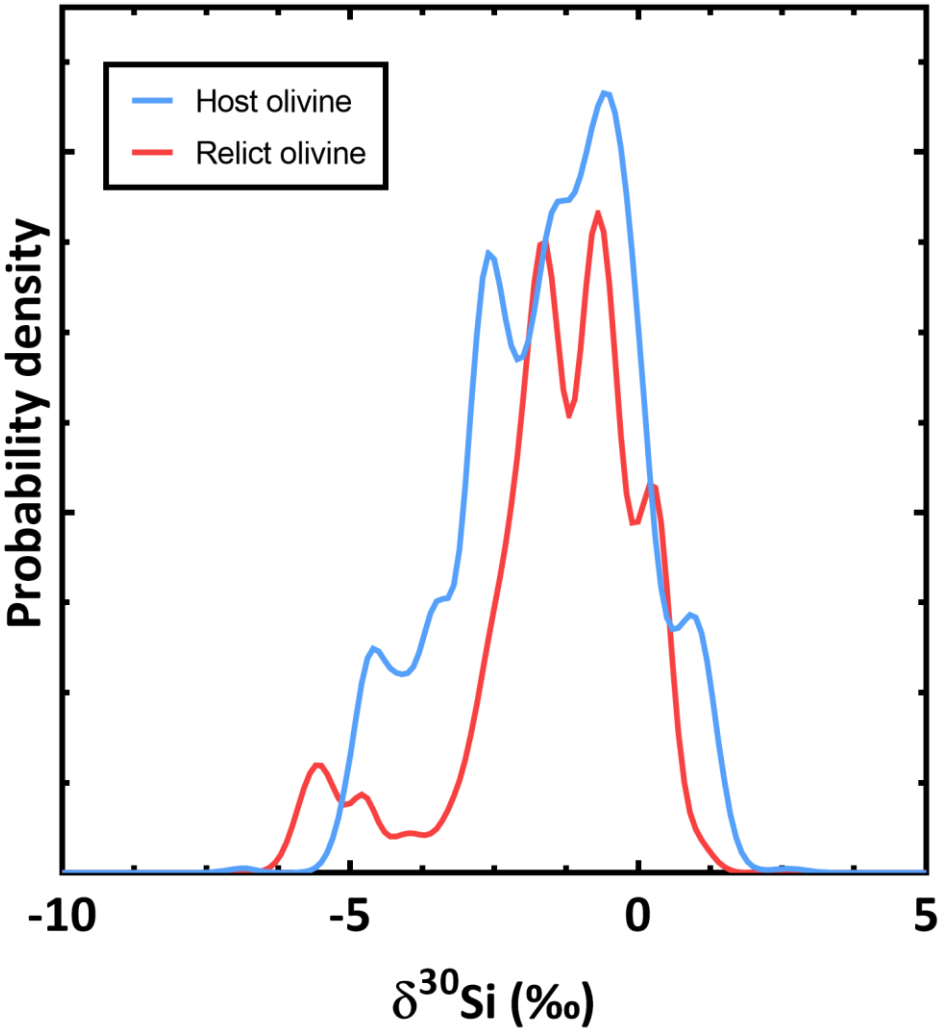
461  
462  
463





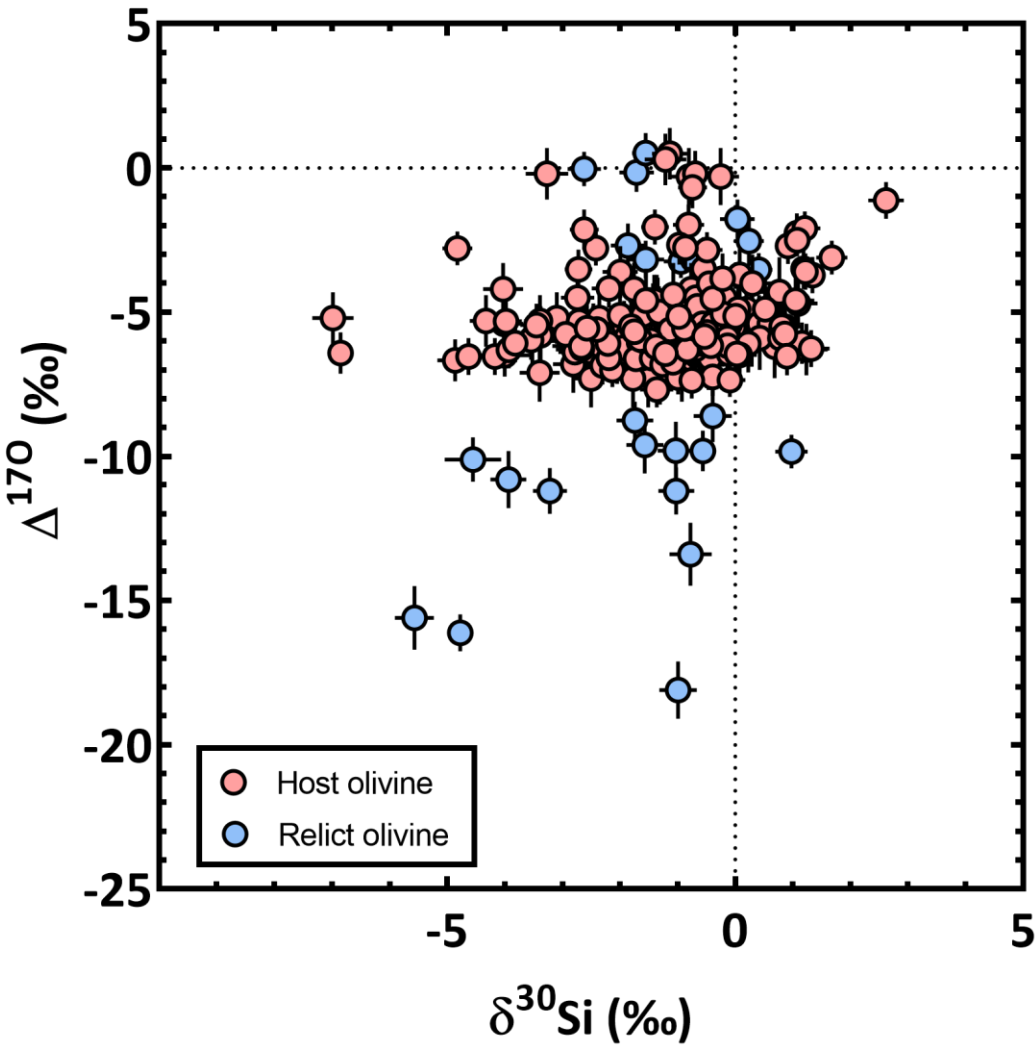
465  
466  
467

468 Fig. 6



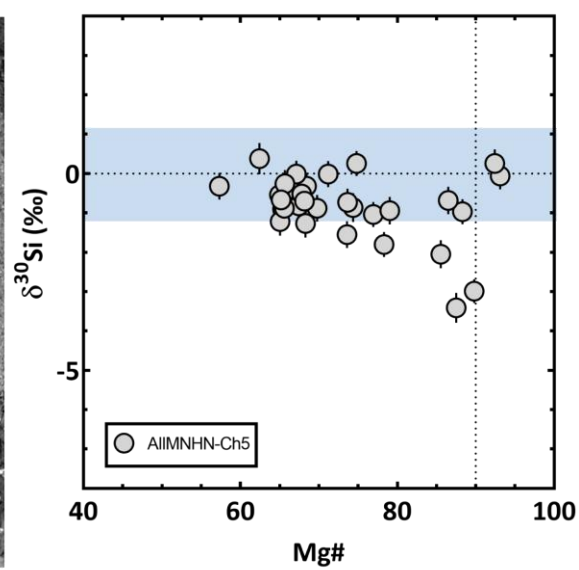
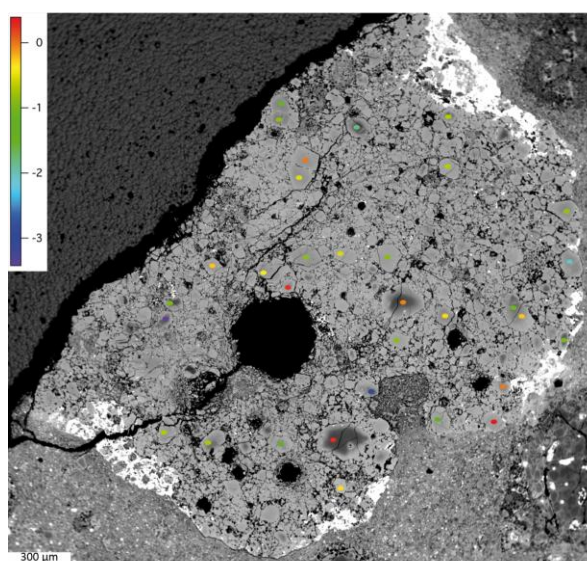
469  
470  
471

472 Fig. 7



473  
474  
475

476 Fig. 8



477